Failure Probability Estimation of a Class of Series Systems by Multidomain Line Sampling

Marcos A. Valdebenito[a,*], Pengfei Wei[b,d], Jingwen Song[c,d], Michael Beer[d,e,f], Matteo Broggi[d]

[a]*Faculty of Engineering and Sciences, Universidad Adolfo Ibáñez, Av. Padre Hurtado 750, 2562340 Viña del Mar, Chile*

[b]*School of Mechanics, Civil Engineering and Architecture, Northwestern Polytechnical University, Xi'an 710072, China*

[c]*Advanced Research Laboratories, Tokyo City University, 1-28-1 Tamazutsumi Setagaya-ku, Tokyo 158-8557, Japan*

[d]*Institute for Risk and Reliability, Leibniz Universität Hannover, Callinstr. 34, 30167 Hannover, Germany*

[e]*Institute for Risk and Uncertainty and School of Engineering, University of Liverpool, Peach Street, Liverpool L69 7ZF, UK*

[f]*International Joint Research Center for Engineering Reliability and Stochastic Mechanics, Tongji University, 1239 Siping Road, Shanghai 200092, P.R. China*

Abstract

This contribution proposes an approach for the assessment of the failure probability associated with a particular class of series systems. The type of systems considered involves components whose response is linear with respect to a number of Gaussian random variables. Component failure occurs whenever this response exceeds prescribed deterministic thresholds. We propose multidomain Line Sampling as an extension of the classical Line Sampling to work with a large number of components at once. By taking advantage of the linearity of the performance functions involved, multidomain Line Sampling explores the interactions that occur between failure domains associated with individual components in order to produce an estimate of the failure probability. The performance and effectiveness of multidomain Line Sampling is illustrated by means of two test problems and an application example, indicating that this technique is amenable for treating problems comprising both a large number of random variables and a large number of components.

Keywords: Line sampling, Multidomain, Linear performance function, Failure probability, Series system

[*]E-mail: marcos.valdebenito@uai.cl

Highlights:

- Failure probability of series system is calculated by multidomain Line Sampling.
- Knowledge on individual component failure domains is exploited.
- Several important directions are considered simultaneously.
- Lines explore interaction between failure events associated with components.

1. Introduction

An engineering system can be seldom described precisely, as different sources of uncertainty may affect its performance. Whenever the nature of uncertainty is of the aleatory type, it is possible to resort to probability theory for analyzing such system [1]. In this way, some input parameters of the system are modeled as random variables (or random processes or random fields, in case time or spatial correlations are present). In turn, such description of the uncertain input parameters causes that the performance of the system becomes random as well. Due to design, operation or maintenance purposes, it is of interest assessing the level of safety associated with the performance of a system, for example, in terms of a failure probability, that measures the chances of an undesirable behavior. At this point, it should be noted that an engineering system usually comprises a number of components, each of which may possess a different failure probability and whose performance may be correlated with that of other components. Depending on the configuration of those components within the system, it may be of interest calculating the failure probability associated with different types of system events: simultaneous failure of all components of the system (parallel event), failure of one or more components (series event), etc. Often, quantifying such failure probability is far from trivial and hence, a number of specialized approaches have been developed for calculating it, for example: bounds based on failure probabilities of individual components and interactions between two [2] or three components [3]; application of surrogate models [4, 5, 6, 7, 8]; linear programming [9, 10, 11] or binary programming [12] techniques; approximation concepts by compounding individual component failure events [13, 14, 15], sampling approaches [16, 17, 18, 19, 20], etc. Although the previous list of contributions is far from being extensive, it demonstrates that calculation of failure probabilities involving different system events is a field of active research.

This contribution focuses on the calculation of the failure probability associated with a series event of a system. In other words, the objective is calculating the probability that the performance of one or more components of a system exceeds a prescribed threshold level. The class of problems considered herein pertain components whose response is characterized as a linear combination of Gaussian random variables. Failure of the component occurs whenever the response falls below a prescribed lower threshold or exceeds a prescribed upper threshold. This class of problems has attracted considerable attention in the literature due to its applications in, e.g. reliability of time-variant systems [21, 22, 23], stochastic linear dynamics [24, 25], seismic fragility analysis [10], geotechnical applications [26, 27], network analysis [28], etc. The focus is on problems that involve a large number of random variables and a large number of components, possibly in the order of thousands.

It should be noted that the type of problems considered in this contribution possesses a distinctive geometry in the standard Gaussian space, where the boundary of the failure domain involves a number of hyperplanes [24]. Such distinctive geometry has allowed to design simulation schemes that allow calculating the sought failure probability with high accuracy and efficiency using either concepts of Importance Sampling [29], Domain Decomposition with averages [30] and Directional Importance Sampling [31, 32]. This work builds on that knowledge of the failure domain and proposes multidomain Line Sampling (mLS), which is a novel extension of Line Sampling [33, 34]. The salient feature of mLS is that it is capable of dealing with failure domains associated with multiple components. This is achieved by introducing multiple search directions instead of a single search direction as usually considered in classical Line Sampling. In addition, lines simulated during the calculation of probability are conditioned to lie in the failure domain, which allows exploring the interaction between failure events associated with individual components along that line.

The rest of this work is organized as follows. Section 2 formulates the failure probability problem associated with a series event of a system. Section 3 presents the description and formulation of multidomain Line Sampling. Section 4 illustrates the application of multidomain Line Sampling to two test problems and an application example, the latter involving a large number of random variables and components. The paper closes with a conclusions and outlook for future developments in Section 5.

2. Formulation of the Problem

2.1. General Aspects

Consider a series system involving a total of n_c components. The behavior of each of these components is described in terms of a response $r_i(\boldsymbol{x}),\ i=1,\ldots,n_c$, that depends on a parameter vector $\boldsymbol{x}$ of dimension n. The component exhibits an acceptable behavior whenever its response lies within prescribed thresholds, that is $b_i^L < r_i(\boldsymbol{x}) < b_i^U$. In other words, failure of the component occurs whenever the response either falls below b_i^L or exceeds b_i^U. Note that no particular restrictions must be imposed regarding the thresholds other than $b_i^L < b_i^U,\ i=1,\ldots,n_c$.

It is assumed that the parameter vector $\boldsymbol{x}$ is uncertain and is characterized by means of a random variable vector $\boldsymbol{X}$ that follows a Gaussian multivariate distribution with mean $\boldsymbol{\mu}$ and (positive definite) covariance matrix $\boldsymbol{C}$. The parameter vector $\boldsymbol{x}$ can be represented in the standard Gaussian space as:

$$\boldsymbol{x} = \boldsymbol{\mu} + \boldsymbol{B}\boldsymbol{z} \tag{1}$$

where $\boldsymbol{z}$ is a realization of $\boldsymbol{Z}$, which follows an n-dimensional standard Gaussian distribution; and where $\boldsymbol{B}$ is a matrix that can be calculated, for example, using Cholesky decomposition or spectral representation. In case the latter is applied, it is noted that $\boldsymbol{B} = \boldsymbol{\Phi}\boldsymbol{\Lambda}^{1/2}$, where the columns of matrix $\boldsymbol{\Phi}$ contain the eigenvectors of $\boldsymbol{C}$ while the diagonal of matrix $\boldsymbol{\Lambda}$ contains the corresponding eigenvalues of $\boldsymbol{C}$. It is further assumed that the response associated with each component depends linearly on $\boldsymbol{x}$, that is $r_i(\boldsymbol{x}) = \boldsymbol{a}_i^T\boldsymbol{x}$, where $\boldsymbol{a}_i$ is an n-dimensional vector with real entries and $(\cdot)^T$ denotes transpose.

Taking into account the previous assumptions, it is possible to formulate two performance functions associated with the i-th component: one for monitoring whenever the response falls below the threshold b_i^L and the other one for monitoring whenever the response exceeds the threshold b_i^U. These functions are equal to:

$$g_{2i-1}(\boldsymbol{z}) = \beta_i^L + \boldsymbol{\alpha}_i^T\boldsymbol{z},\ i=1,\ldots,n_c \tag{2}$$

$$g_{2i}(\boldsymbol{z}) = \beta_i^U - \boldsymbol{\alpha}_i^T\boldsymbol{z},\ i=1,\ldots,n_c \tag{3}$$

where $\beta_i^L = \left(\boldsymbol{a}_i^T\boldsymbol{\mu} - b_i^L\right)/||\boldsymbol{a}_i^T\boldsymbol{B}||$, $\beta_i^U = \left(b_i^U - \boldsymbol{a}_i^T\boldsymbol{\mu}\right)/||\boldsymbol{a}_i^T\boldsymbol{B}||$, $\boldsymbol{\alpha}_i = \boldsymbol{a}_i^T\boldsymbol{B}/||\boldsymbol{a}_i^T\boldsymbol{B}||$ and $||\cdot||$ denotes Euclidean norm. Note that the formulation of the performance function in eq. (2) is actually equal to the subtraction between the response r_i (which has been expressed in terms of vector $\boldsymbol{z}$ applying eq. (1)) and the threshold b_i^L, divided by the Euclidean norm of vector $\boldsymbol{a}_i^T \boldsymbol{B}$. This ensures that $g_{2i-1}(\boldsymbol{z})$ assumes a value equal or smaller than zero whenever the response equals or is below the threshold b_i^L. In a similar way, eq. (3) is constructed as the subtraction between the threshold level b_i^U and the response r_i, divided by the Euclidean norm of vector $\boldsymbol{a}_i^T \boldsymbol{B}$. Thus, $g_{2i}(\boldsymbol{z})$ assumes a value equal or smaller than zero whenever the response equals or exceeds the threshold b_i^U. Note that in the previous definitions of the performance functions, normalization by the Euclidean norm of vector $\boldsymbol{a}_i^T \boldsymbol{B}$ is enforced as this ensures that $||\boldsymbol{\alpha}_i|| = 1,\ i = 1, \ldots, n_c$.

2.2. Failure Probability Associated with Individual Component

Different realizations $\boldsymbol{z}$ of the random vector $\boldsymbol{Z}$ may cause failure of the i-th component. The set of all of these realizations is denoted as the failure domain F_i. In turn, this failure domain is the union of a negative (F_i^-) and a positive failure domain (F_i^+), that is $F_i = F_i^- \cup F_i^+$. The negative failure domain F_i^- is a set that groups all realizations $\boldsymbol{z}$ such that the response of the i-th component is equal to or below the threshold b_i^L, that is $F_i^- = \{\boldsymbol{z} \in \mathbb{R}^n : g_{2i-1}(\boldsymbol{z}) \leq 0\}$, $i = 1, \ldots, n_c$. In a similar way, the positive elementary failure domain F_i^+ groups all realizations $\boldsymbol{z}$ such that the response of the i-th component is equal to or exceeds the threshold b_i^U, that is $F_i^+ = \{\boldsymbol{z} \in \mathbb{R}^n : g_{2i}(\boldsymbol{z}) \leq 0\}$, $i = 1, \ldots, n_c$. In view of the linearity of each of the performance functions g_i with respect to $\boldsymbol{z}$ as noted from eqs. (2) and (3), negative and positive failure domains are bounded by hyperplanes. Furthermore, the negative and positive failure domains are fully described by their corresponding design points. Recall that the design point $\boldsymbol{z}^*$ is the realization of $\boldsymbol{Z}$ with smallest Euclidean norm with respect to the origin that causes failure. It is straightforward to demonstrate that the design points associated with each performance function are equal to $\boldsymbol{z}^*_{2i-1} = -\beta_i^L \boldsymbol{\alpha}_i$ and $\boldsymbol{z}^*_{2i} = \beta_i^U \boldsymbol{\alpha}_i,\ i = 1, \ldots, n_c$, respectively [24, 29]. Figure 1 provides a schematic representation of the negative and positive failure domains as well as their corresponding design points for the specific case where $n = 2$ and $n_c = 1$.

The probability of failure of the i-th component is denoted as $p_{F,i}$ and is defined as:

$$p_{F,i} = \int_{\boldsymbol{z} \in \mathbb{R}^n} I_{F_i}(\boldsymbol{z}) f_{\boldsymbol{Z}}(\boldsymbol{z}) d\boldsymbol{z} \tag{4}$$

where $f_{\boldsymbol{Z}}(\boldsymbol{z})$ is the standard Gaussian probability density function in n dimensions; and where $I_{F_i}(\boldsymbol{z})$ is the indicator function associated with the i-the failure event, which is equal to $I_{F_i}(\boldsymbol{z}) = 1$

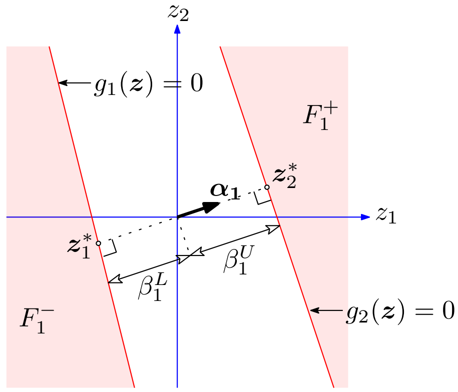

Figure 1: Schematic representation of negative and positive failure domains (F_i^- and F_i^+, respectively) and their design points ($n = 2,\ n_c = 1$).

in case $\boldsymbol{z} \in F_i$ and zero, otherwise. In view of the linearity of the performance functions g_{2i-1} and g_{2i} with respect to $\boldsymbol{z}$, the probability integral in eq. (4) possesses an analytic solution [2], which is equal to:

$$p_{F,i} = \Phi\left(-\beta_i^L\right) + \Phi\left(-\beta_i^U\right) \tag{5}$$

where $\Phi(\cdot)$ is the standard Gaussian cumulative density function. Note that β_i^L and β_i^U are actually the reliability indexes associated with F_i^- and F_i^+, respectively [2, 24]. In other words, they are the Euclidean norm of the corresponding design points, that is $\beta_i^L = ||\boldsymbol{z}_{2i-1}^*||$ and $\beta_i^U = ||\boldsymbol{z}_{2i}^*||$, $i = 1, \ldots, n_c$ [24].

2.3. Failure Probability Associated with Series Event

The failure event associated with a series system implies that one or more of its components fail. The failure domain F groups all realizations $\boldsymbol{z}$ of the random variable vector $\boldsymbol{Z}$ that cause the failure event, that is, $F = F_1 \cup F_2 \cup \ldots \cup F_{n_c}$. The probability of failure associated with the systems event is denoted as p_F and is defined as:

$$p_F = \int_{\boldsymbol{z}\in\mathbb{R}^n} I_F(\boldsymbol{z}) f_{\boldsymbol{Z}}(\boldsymbol{z}) d\boldsymbol{z} \tag{6}$$

where $I_F(\boldsymbol{z})$ is the indicator function, which is equal to $I_F(\boldsymbol{z}) = 1$ in case $\boldsymbol{z} \in F$ and zero, otherwise. It is important to note that for most cases of practical interest, eq. (6) cannot be solved in closed form [13]. This is due to the fact that interactions between the failure domains associated with individual components cannot be analyzed analytically. In addition to the issue of interactions, the number of random variables n and of performance functions n_c associated with the probability integral may be considerable (in the order of hundreds or thousands). These two issues favor the application of simulation methods for calculating the failure probability [35].

3. Multidomain Line Sampling

3.1. Line Sampling

Line Sampling is a simulation technique which was developed for calculating failure probabilities in problems involving a large number of random variables [33, 36]. It is closely related to another simulation technique known as Axis Orthogonal Sampling [37, 38]. Most of the applications of Line Sampling which are available in the literature focus on the assessment of failure probabilities associated with weakly or moderately nonlinear performance functions of an individual component, see e.g. [39].

The practical implementation of Line Sampling requires that the reliability problem is formulated in the standard Gaussian space by means of a suitable projection [40]. After that, it is necessary to identify the so-called *important direction* $\boldsymbol{\gamma}$, which is a vector of unit Euclidean norm located at the origin of the standard normal space that points towards the failure domain. Several criteria have been proposed for determining such direction [33, 41]. Then, taking advantage of the rotational invariance of the standard Gaussian distribution, a rotated coordinate system is introduced, such that:

$$\boldsymbol{z} = \boldsymbol{R}\boldsymbol{z}^{\perp} + \boldsymbol{\gamma} z^{\parallel} \tag{7}$$

where $\boldsymbol{z}^{\perp}$ is a vector of dimension $(n-1)$ that represents coordinates in the hyperplane orthogonal to $\boldsymbol{\gamma}$; $z^{\parallel}$ is a scalar denoting the coordinate parallel to $\boldsymbol{\gamma}$; and $\boldsymbol{R}$ is a matrix of dimension $n \times (n-1)$. The square matrix $[\boldsymbol{R}, \boldsymbol{\gamma}]$ forms an orthonormal basis and thus, it is straightforward to demonstrate that $z^{\parallel} = \boldsymbol{\gamma}^T \boldsymbol{z}$ and $\boldsymbol{z}^{\perp} = \boldsymbol{R}^T \boldsymbol{z}$. Note that for practical implementation, there is no need to determine matrix $\boldsymbol{R}$ in explicit form. In addition, note that the probability distributions associated with $\boldsymbol{z}^{\perp}$ and $z^{\parallel}$ are standard Gaussian distributions in $(n-1)$ dimensions and one dimension, respectively.

Line Sampling takes advantage of the rotated coordinate system associated with eq. (7) by combining simulation with numerical integration. That is, random samples are generated in the hyperplane orthogonal to the important direction $\boldsymbol{\gamma}$. These samples are denoted as $\boldsymbol{z}^{\perp,(j)}$, $j = 1, \ldots, N$, where N denotes the number of samples. Then, one-dimensional numerical integration is performed along the line $l^{(j)}$, $j = 1, \ldots, N$, that is parallel to the important direction and that contains the sample $\boldsymbol{z}^{\perp,(j)}$. The aim of this one-dimensional integration is determining which portions of the line contribute to the failure probability integral. The whole procedure is depicted schematically in Figure 2, where the dimension of the problem is $n = 2$ and the number of lines is set equal to $N = 2$. Note that in this figure, the performance function is denoted as $g(\boldsymbol{z})$.

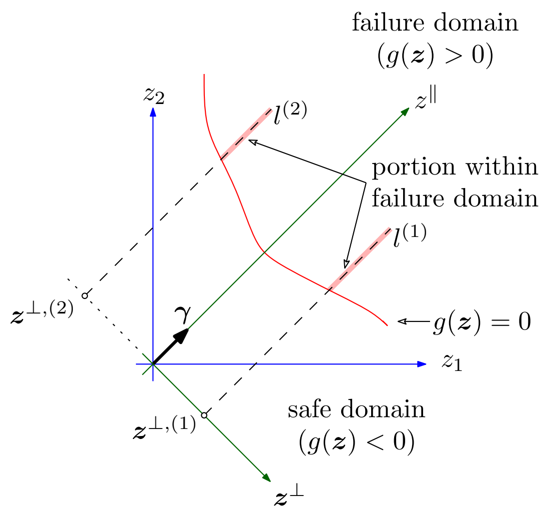

Figure 2: Schematic representation of Line Sampling considering two lines ($n = N = 2$).

3.2. *Formulation of multidomain Line Sampling*

Recall that the objective of this work is formulating a simulation scheme for calculating failure probabilities of series systems involving a large number of components whose performance functions are linear with respect to a set of parameters following a Gaussian distribution. In order to develop such simulation scheme, note that the summation of the failure probabilities of individual components provides an upper bound for the failure probability of the series event, that is $p_F \leq p_{F,1} + p_{F,2} + \ldots + p_{F,n_c}$ [2, 29]. Such inequality can be understood with the help of the schematic representation in Figure 3, where it is assumed for simplicity that $n = n_c = 2$. When examining this figure, it is noted that failure domains associated with components F_1 and F_2 exhibit overlap; in fact, this overlap occurs at each of the four corners of the figure, that is $F_1^+ \cap F_2^+$ (upper-right corner), $F_1^+ \cap F_2^-$ (lower-right corner), $F_1^- \cap F_2^-$ (lower-left corner) and $F_1^- \cap F_2^+$ (upper-left corner). This implies that the quantity $p_{F,1} + p_{F,2}$ must be necessarily larger than p_F, as the probability content associated with those overlapping regions is being counted twice. In other words, direct summation of the probabilities of failure of individual components does not take into account the possible interactions between the failure domains associated with each component, which in Figure 3 correspond to the realizations of $\boldsymbol{z}$ that belong to any of the sets $F_1^+ \cap F_2^+$, $F_1^+ \cap F_2^-$, $F_1^- \cap F_2^-$ and $F_1^- \cap F_2^+$.

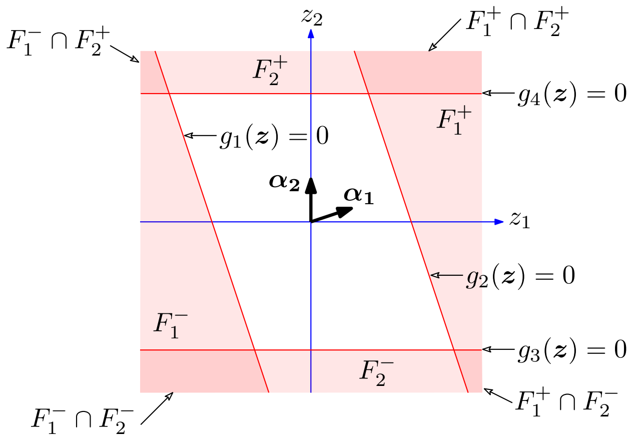

Figure 3: Schematic representation of failure domains associated with components ($n = n_c = 2$).

The overlap between failure domains associated with individual components can be taken into account by explicitly modeling their interaction [29, 30]. For that purpose, let p_i be equal to:

$$p_i = \int_{\boldsymbol{z} \in F_i} \frac{1}{\sum_{k=1}^{n_c} I_{F_k}(\boldsymbol{z})} f_{\boldsymbol{Z}}(\boldsymbol{z}) d\boldsymbol{z}, i = 1, \ldots, n_c \tag{8}$$

Note that p_i is the integral over the set F_i of the standard Gaussian probability density function divided by the sum of individual failure events that are associated with a particular realization $\boldsymbol{z}$. Clearly, p_i as defined in eq. (8) is different from the probability of failure of the i-th component $p_{F,i}$ (see eq. (4)). In fact, the quantity p_i can be loosely interpreted as the *effective* contribution of the i-th component to the failure probability associated with the series event, where interaction with other components is discounted by means of the factor $1/\sum_{k=1}^{n_c} I_{F_k}(\boldsymbol{z})$. It is readily seen that:

$$\begin{aligned}
\sum_{i=1}^{n_c} p_i &= \sum_{i=1}^{n_c} \left(\int_{\boldsymbol{z} \in F_i} \frac{1}{\sum_{k=1}^{n_c} I_{F_k}(\boldsymbol{z})} f_{\boldsymbol{Z}}(\boldsymbol{z}) d\boldsymbol{z} \right) \\
&= \sum_{i=1}^{n_c} \left(\int_{\boldsymbol{z} \in F} \frac{I_{F_i}(\boldsymbol{z})}{\sum_{k=1}^{n_c} I_{F_k}(\boldsymbol{z})} f_{\boldsymbol{Z}}(\boldsymbol{z}) d\boldsymbol{z} \right) \\
&= \int_{\boldsymbol{z} \in F} \frac{\sum_{i=1}^{n_c} I_{F_i}(\boldsymbol{z})}{\sum_{k=1}^{n_c} I_{F_k}(\boldsymbol{z})} f_{\boldsymbol{Z}}(\boldsymbol{z}) d\boldsymbol{z} \\
&= \int_{\boldsymbol{z} \in F} f_{\boldsymbol{Z}}(\boldsymbol{z}) d\boldsymbol{z} = \int_{\boldsymbol{z} \in \mathbb{R}^n} I_F(\boldsymbol{z}) f_{\boldsymbol{Z}}(\boldsymbol{z}) d\boldsymbol{z} = p_F
\end{aligned} \tag{9}$$

which implies that the summation of all $p_i,\ i=1,\ldots,n_c$ is equal to the failure probability p_F. For a better understanding of the above equation, consider again Figure 3. The quantity p_1 would be equal to the integral of the standard Gaussian probability density function over the set $F_1 \setminus F_2$ (where $(\cdot)\setminus(\cdot)$ denotes set subtraction) plus one half of the standard Gaussian probability distribution over set $F_1 \cap F_2$. In a similar way, p_2 would be equal to the integral of the standard Gaussian probability density function over the set $F_2 \setminus F_1$ plus one half of the standard Gaussian probability distribution over set $F_1 \cap F_2$. Clearly, the summation of p_1 and p_2 would be equal to p_F, as in this case, the interaction between components has been accounted for by means of the factor $1/\sum_{k=1}^{n_c} I_{F_k}(\boldsymbol{z})$.

The calculation of the probability of failure of a series event as proposed in eq. (9) demands calculating the quantities $p_i,\ i=1,\ldots,n_c$. These quantities can be evaluated by means of Line Sampling. For that purpose, consider the failure domain associated with the i-th component: an obvious choice for the important direction would be $\boldsymbol{\gamma} = \boldsymbol{\alpha}_i$. Then, a rotated coordinate system is introduced such that:

$$\boldsymbol{z} = \boldsymbol{R}_i \boldsymbol{z}_i^{\perp} + \boldsymbol{\alpha}_i z_i^{\parallel} \tag{10}$$

where $\boldsymbol{z}_i^{\perp}$ and $z_i^{\parallel}$ denote the set of coordinates which are orthogonal and parallel to $\boldsymbol{\alpha}_i$, respectively; and where $\boldsymbol{R}_i$ denotes the corresponding matrix for coordinate rotation. Figure 4 provides a schematic illustration of the different rotated coordinate systems for a case where $n = n_c = 2$.

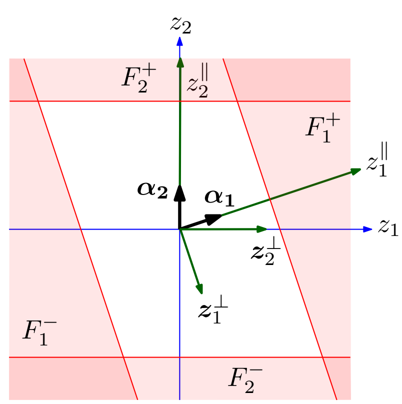

Figure 4: Schematic representation of multidomain Line Sampling considering two rotated coordinate systems ($n = n_c = 2$).

Assuming that the square matrix $[\boldsymbol{R}_i, \boldsymbol{\alpha}_i]$ forms an orthonormal basis, the probability distributions associated with $\boldsymbol{z}_i^{\perp}$ and $z_i^{\parallel}$ are standard Gaussian in $(n-1)$ dimensions and one dimension, respectively. Thus, taking into account eqs. (8) and (10), the integral associated with the quantity

p_i is recast as:

$$p_i = \int_{\boldsymbol{z}_i^{\perp} \in \mathbb{R}^{n-1}} \int_{\left(z_i^{\parallel}, \boldsymbol{z}_i^{\perp}\right) \in F_i} \frac{1}{\sum_{k=1}^{n_c} I_{F_k}\left(\boldsymbol{R}_i \boldsymbol{z}_i^{\perp} + \boldsymbol{\alpha}_i z_i^{\parallel}\right)} f_{Z_i^{\parallel}}\left(z_i^{\parallel}\right) f_{\boldsymbol{Z}_i^{\perp}}\left(\boldsymbol{z}_i^{\perp}\right) dz_i^{\parallel} d\boldsymbol{z}_i^{\perp},\ i = 1, \ldots, n_c \quad (11)$$

The last equation can be further simplified by taking into account that the performance functions associated with the i-th failure domain in the rotated coordinates are equal to $g_{2i-1}\left(z_i^{\parallel}, \boldsymbol{z}_i^{\perp}\right) = \beta_i^L + z_i^{\parallel}$ and $g_{2i}\left(z_i^{\parallel}, \boldsymbol{z}_i^{\perp}\right) = \beta_i^U - z_i^{\parallel}$, yielding:

$$\begin{aligned} p_i = & \int_{\boldsymbol{z}_i^{\perp} \in \mathbb{R}^{n-1}} \int_{-\infty}^{-\beta_i^L} \frac{1}{\sum_{k=1}^{n_c} I_{F_k}\left(\boldsymbol{R}_i \boldsymbol{z}_i^{\perp} + \boldsymbol{\alpha}_i z_i^{\parallel}\right)} f_{Z_i^{\parallel}}\left(z_i^{\parallel}\right) f_{\boldsymbol{Z}_i^{\perp}}\left(\boldsymbol{z}_i^{\perp}\right) dz_i^{\parallel} d\boldsymbol{z}_i^{\perp} + \\ & \int_{\boldsymbol{z}_i^{\perp} \in \mathbb{R}^{n-1}} \int_{\beta_i^U}^{\infty} \frac{1}{\sum_{k=1}^{n_c} I_{F_k}\left(\boldsymbol{R}_i \boldsymbol{z}_i^{\perp} + \boldsymbol{\alpha}_i z_i^{\parallel}\right)} f_{Z_i^{\parallel}}\left(z_i^{\parallel}\right) f_{\boldsymbol{Z}_i^{\perp}}\left(\boldsymbol{z}_i^{\perp}\right) dz_i^{\parallel} d\boldsymbol{z}_i^{\perp},\ i = 1, \ldots, n_c \end{aligned} \quad (12)$$

The above equation provides an expression for calculating p_i within the framework of Line Sampling. As integration along the parallel direction is carried out taking into account interactions of the failure events associated with the different components, eq. (12) is denoted as a *multidomain Line Sampling* (mLS) expression for calculating p_i.

Direct calculation of the expression for the failure probability as proposed in eq. (9) demands calculating each individual quantity $p_i,\ i = 1, \ldots, n_c$ by means of mLS. As it is expected that n_c can be in the order of hundreds or even thousands, calculating each term in the summation can become extremely demanding. As an alternative, this summation can be estimated by means of simulation, following the approach proposed in [30]. For that purpose, consider the following variant of eq. (9):

$$p_F = \sum_{i=1}^{n_c} \left(\frac{1}{\omega_i} p_i\right) \omega_i \quad (13)$$

where $\omega_i,\ i = 1, \ldots, n_c$ is a weight factor such that $\omega_i > 0$ and $\sum_{i=1}^{n_c} \omega_i = 1$. This set of weights can be interpreted as the probability mass function of a discrete random variable. A possible criterion for selecting the i-th weight is to set it proportional to the failure probability associated with the i-th component, as considered in Importance Sampling using design points [42]. This leads to the following expression for calculating the weights.

$$\omega_i = \frac{p_{F,i}}{\sum_{k=1}^{n_c} p_{F,k}}, \; i = 1, \ldots, n_c \tag{14}$$

Thus, eq. (13) becomes an expression that involves summation over a discrete random variable as well as integration over a number of continuous random variables. Within the context of simulation, p_F is estimated by generating samples of the discrete and continuous random variables, that is:

$$p_F \approx \tilde{p}_F = \frac{1}{N} \sum_{j=1}^{N} \left(\frac{1}{\omega_{i(j)}} p_{i^{(j)}} \left(\boldsymbol{z}_{i(j)}^{\perp,(j)} \right) \right) \tag{15}$$

where $\tilde{p}_F$ is an estimate of p_F; N denotes the total number of samples; $i^{(j)}, \; j = 1, \ldots, N$ are independent and identically distributed samples drawn with replacement from the set $I = \{1, 2, \ldots, n_c\}$ with probability mass function $\omega_i, \; i = 1, \ldots, n_c$; $\boldsymbol{z}_{i(j)}^{\perp,(j)}, \; j = 1, \ldots, N$ are independent and identically distributed samples that follow $f_{\boldsymbol{Z}_{i(j)}^{\perp}} \left(\boldsymbol{z}_{i(j)}^{\perp} \right)$; and where $p_{i^{(j)}} \left(\boldsymbol{z}_{i(j)}^{\perp,(j)} \right), \; j = 1, \ldots, N$ represents an estimate of quantity $p_{i^{(j)}}$ evaluated at the sample $\boldsymbol{z}_{i(j)}^{\perp,(j)}$, that is:

$$\begin{aligned} p_{i^{(j)}} \left(\boldsymbol{z}_{i(j)}^{\perp,(j)} \right) = & \int_{-\infty}^{-\beta_{i(j)}^{L}} \frac{1}{\sum_{k=1}^{n_c} I_{F_k} \left(\boldsymbol{R}_{i(j)} \boldsymbol{z}_{i(j)}^{\perp,(j)} + \boldsymbol{\alpha}_{i(j)} z_{i(j)}^{\parallel} \right)} f_{Z_{i(j)}^{\parallel}} \left(z_{i(j)}^{\parallel} \right) dz_{i(j)}^{\parallel} + \\ & \int_{\beta_{i(j)}^{U}}^{\infty} \frac{1}{\sum_{k=1}^{n_c} I_{F_k} \left(\boldsymbol{R}_{i(j)} \boldsymbol{z}_{i(j)}^{\perp,(j)} + \boldsymbol{\alpha}_{i(j)} z_{i(j)}^{\parallel} \right)} f_{Z_{i(j)}^{\parallel}} \left(z_{i(j)}^{\parallel} \right) dz_{i(j)}^{\parallel}, \; j = 1, \ldots, N \end{aligned} \tag{16}$$

It is seen that the last equation corresponds to an estimate of the quantity p_i calculated by means of mLS. It represents the integral over the line that passes through the sample $\boldsymbol{z}_{i(j)}^{\perp,(j)}$ and which is parallel to $\boldsymbol{\alpha}_{i(j)}$ and whose argument is the standard Gaussian univariate probability distribution divided over the number of components that fail at a given point of that line. Thus, eq. (16) can be interpreted as a means of exploring the interactions that occur between the behavior of different components along the line. Details about the numerical evaluation of eq. (16) are discussed in Section 3.3.2.

It is straightforward to demonstrate that the coefficient of variation of the probability estimate of eq. (15) (which is denoted as δ_{p_F}) is equal to:

$$\delta_{p_F} = \frac{1}{\tilde{p}_F}\sqrt{\frac{1}{N(N-1)}\sum_{j=1}^{N}\left(\left(\frac{1}{\omega_{i(j)}}p_{i(j)}\left(\boldsymbol{z}_{i(j)}^{\perp,(j)}\right)\right)-\tilde{p}_F\right)^2} \tag{17}$$

3.3. Practical Implementation

Practical implementation of eq. (16) demands solving two issues: the generation of samples $\boldsymbol{z}_{i(j)}^{\perp,(j)},\ j=1,\ldots,N$ and the calculation of the line integral associated with mLS. These two issues are discussed in the following.

3.3.1. Generation of samples $\boldsymbol{z}_{i(j)}^{\perp,(j)}$

Regarding the first implementation issue, recall that $\boldsymbol{z}_{i(j)}^{\perp,(j)},\ j=1,\ldots,N$ are independent and identically distributed samples that follow $f_{\boldsymbol{Z}_{i(j)}^{\perp}}\left(\boldsymbol{z}_{i(j)}^{\perp}\right)$. These samples can be conveniently generated by means of the following algorithm.

1. Set $j=1$.
2. Draw an element from the set $I=\{1,2,\ldots,n_c\}$ with probability $\omega_i,\ i=1,\ldots,n_c$. The drawn element is denoted as $i^{(j)}$.
3. Generate a random sample $\boldsymbol{z}^{(j)}$ following a n-dimensional standard Gaussian distribution.
4. Calculate [33, 34]:
$$\boldsymbol{R}_{i(j)}\boldsymbol{z}_{i(j)}^{\perp,(j)} = \boldsymbol{z}^{(j)} - \left(\boldsymbol{\alpha}_{i(j)}^T\boldsymbol{z}^{(j)}\right)\boldsymbol{\alpha}_{i(j)} \tag{18}$$
5. In case $j=N$, stop the algorithm. Otherwise, return to step 2 with $j=j+1$.

The core of the algorithm described above lies in step 4, which is represented schematically in Figure 5, where it has been assumed for simplicity that $n=n_c=2$ and that $i^{(j)}=1$. As noted from Figure 5, eq. (18) consists of subtracting the projection of the random sample $\boldsymbol{z}^{(j)}$ over the important direction $\boldsymbol{\alpha}_{i(j)}$ (that is, $\left(\boldsymbol{\alpha}_{i(j)}^T\boldsymbol{z}^{(j)}\right)\boldsymbol{\alpha}_{i(j)}$) from the random sample $\boldsymbol{z}^{(j)}$ itself [33, 34]. It should be noted that such step does not produce $\boldsymbol{z}_{i(j)}^{\perp,(j)}$ but instead, it leads to $\boldsymbol{R}_{i(j)}\boldsymbol{z}_{i(j)}^{\perp,(j)}$. This is quite convenient from a numerical viewpoint, as all calculations associated with mLS demand knowledge of $\boldsymbol{R}_{i(j)}\boldsymbol{z}_{i(j)}^{\perp,(j)}$ (and not of $\boldsymbol{z}_{i^{\perp,(j)}}$). Hence, explicit calculation of the rotation matrices $\boldsymbol{R}_i,\ i=1,\ldots,n_c$ is avoided.

3.3.2. Evaluation of integral along line

Eq. (16) corresponds to a one-dimensional integral along the line $l^{(j)}$ that passes through

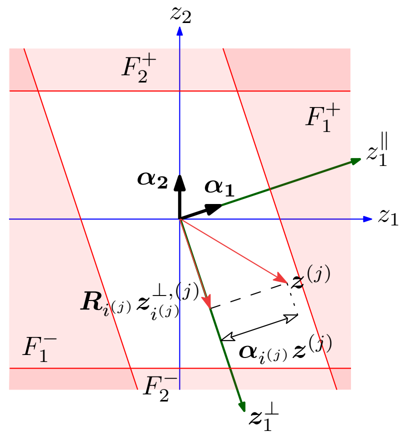

Figure 5: Schematic representation of generation of samples for multidomain Line Sampling ($n = n_c = 2$, $i^{(j)} = 1$).

the sample $\boldsymbol{z}_{i^{(j)}}^{\perp,(j)}$ and which is parallel to $\boldsymbol{\alpha}_{i^{(j)}}$. The argument of this integral is the standard Gaussian probability density function as a function of the coordinate $z_{i^{(j)}}^{\parallel}$ divided by the number of components that fail at realization $\boldsymbol{R}_{i^{(j)}}\boldsymbol{z}_{i^{(j)}}^{\perp,(j)} + \boldsymbol{\alpha}_{i^{(j)}} z_{i^{(j)}}^{\parallel}$; the latter number is given by the formula $\sum_{k=1}^{n_c} I_{F_k}\left(\boldsymbol{R}_{i^{(j)}}\boldsymbol{z}_{i^{(j)}}^{\perp,(j)} + \boldsymbol{\alpha}_{i^{(j)}} z_{i^{(j)}}^{\parallel}\right)$. As $\boldsymbol{R}_{i^{(j)}}\boldsymbol{z}_{i^{(j)}}^{\perp,(j)}$ is a fixed vector for a given line (see eq. (18)), the challenge for calculating the line integral in eq. (16) lies precisely in calculating the number of failed components as a function of $z_{i^{(j)}}^{\parallel}$. For a better understanding of this issue, consider the schematic representation in Figure 6, that depicts a particular case where $n = n_c = 2$, $N = 1$ and $i^{(1)} = 2$. In particular, Figure 6(a) illustrates the problem in the space of standard Gaussian random variables, where $l^{(1)}$ denotes the line that passes through the sample $\boldsymbol{z}_2^{\perp,(1)}$ and which is parallel to $\boldsymbol{\alpha}_2$. It is seen that line $l^{(1)}$ intersects the different failure domains associated with each of the two components considered. Such issue must be considered when solving the integral associated with that line, as this affects the indicator functions of each component $I_{F_k}\left(\boldsymbol{R}_2\boldsymbol{z}_2^{\perp,(1)} + \boldsymbol{\alpha}_2 z_2^{\parallel}\right)$, $k = 1, 2$, as depicted schematically in Figures 6(b) and 6(c), respectively, as well as the compound indicator function $\sum_{k=1}^{2} I_{F_k}\left(\boldsymbol{R}_2\boldsymbol{z}_2^{\perp,(1)} + \boldsymbol{\alpha}_2 z_2^{\parallel}\right)$, as seen in Figure 6(d). A close examination of the indicator functions associated with the components as shown in Figures 6(b) and 6(c) reveals that they can be represented as the summation of two unit step functions. In a general case, the indicator function associated with component k is cast as:

$$\begin{aligned} I_{F_k}\left(\boldsymbol{R}_{i^{(j)}}\boldsymbol{z}_{i^{(j)}}^{\perp,(j)} + \boldsymbol{\alpha}_{i^{(j)}} z_{i^{(j)}}^{\parallel}\right) = u\left(-g_{2k-1}\left(\boldsymbol{R}_{i^{(j)}}\boldsymbol{z}_{i^{(j)}}^{\perp,(j)} + \boldsymbol{\alpha}_{i^{(j)}} z_{i^{(j)}}^{\parallel}\right)\right) + \\ u\left(-g_{2k}\left(\boldsymbol{R}_{i^{(j)}}\boldsymbol{z}_{i^{(j)}}^{\perp,(j)} + \boldsymbol{\alpha}_{i^{(j)}} z_{i^{(j)}}^{\parallel}\right)\right),\ k = 1, \ldots, n_c,\ j = 1, \ldots, N \end{aligned} \quad (19)$$

where $u(\cdot)$ denotes the unit step function. Replacing the expressions for the performance functions

$g_{2k-1}(\boldsymbol{z})$ and $g_{2k}(\boldsymbol{z})$ (see eqs. (2) and (3), respectively) into the above equation leads to the following expression.

$$I_{F_k}\left(\boldsymbol{R}_{i^{(j)}}\boldsymbol{z}_{i^{(j)}}^{\perp,(j)} + \boldsymbol{\alpha}_{i^{(j)}} z_{i^{(j)}}^{\parallel}\right) = u\left(-\beta_k^L - \boldsymbol{\alpha}_k^T \boldsymbol{R}_{i^{(j)}}\boldsymbol{z}_{i^{(j)}}^{\perp,(j)} - \boldsymbol{\alpha}_k^T \boldsymbol{\alpha}_{i^{(j)}} z_{i^{(j)}}^{\parallel}\right) + \\ u\left(-\beta_k^U + \boldsymbol{\alpha}_k^T \boldsymbol{R}_{i^{(j)}}\boldsymbol{z}_{i^{(j)}}^{\perp,(j)} + \boldsymbol{\alpha}_k^T \boldsymbol{\alpha}_{i^{(j)}} z_{i^{(j)}}^{\parallel}\right),\ k = 1,\ldots,n_c,\ j = 1,\ldots,N \tag{20}$$

Under the assumption that $\boldsymbol{\alpha}_k^T \boldsymbol{\alpha}_{i^{(j)}} \neq 0$, it is possible to express the last equation in a more compact format, that is:

$$I_{F_k}\left(\boldsymbol{R}_{i^{(j)}}\boldsymbol{z}_{i^{(j)}}^{\perp,(j)} + \boldsymbol{\alpha}_{i^{(j)}} z_{i^{(j)}}^{\parallel}\right) = u\left(\xi_{2k-1}^{(j)}\left(z_{i^{(j)}}^{\parallel} - c_{2k-1}^{(j)}\right)\right) + u\left(\xi_{2k}^{(j)}\left(z_{i^{(j)}}^{\parallel} - c_{2k}^{(j)}\right)\right), \\ k = 1,\ldots,n_c,\ j = 1,\ldots,N \tag{21}$$

where:

$$c_{2k-1}^{(j)} = -\frac{\beta_k^L + \boldsymbol{\alpha}_k^T \boldsymbol{R}_{i^{(j)}}\boldsymbol{z}_{i^{(j)}}^{\perp,(j)}}{\boldsymbol{\alpha}_k^T \boldsymbol{\alpha}_{i^{(j)}}} \tag{22}$$

$$c_{2k}^{(j)} = \frac{\beta_k^U - \boldsymbol{\alpha}_k^T \boldsymbol{R}_{i^{(j)}}\boldsymbol{z}_{i^{(j)}}^{\perp,(j)}}{\boldsymbol{\alpha}_k^T \boldsymbol{\alpha}_{i^{(j)}}} \tag{23}$$

$$\xi_{2k-1}^{(j)} = -\mathrm{sgn}\left(\boldsymbol{\alpha}_k^T \boldsymbol{\alpha}_{i^{(j)}}\right) \tag{24}$$

$$\xi_{2k}^{(j)} = \mathrm{sgn}\left(\boldsymbol{\alpha}_k^T \boldsymbol{\alpha}_{i^{(j)}}\right) \tag{25}$$

and where $\mathrm{sgn}(\cdot)$ represents the sign function. As noted from eq. (21), $c_{2k-1}^{(j)}$ and $c_{2k}^{(j)}$ denote the coordinate $z_{i^{(j)}}^{\parallel}$ for which the corresponding unit step function changes its value. Such concept is represented schematically in Figures 6(b) and 6(c). In fact, $c_{2k-1}^{(j)}$ and $c_{2k}^{(j)}$ denote the Euclidean distances from the sample $\boldsymbol{z}_{i^{(j)}}^{\perp,(j)}$ to the limit state functions $g_{2k-1}(\boldsymbol{z}) = 0$ and $g_{2k}(\boldsymbol{z}) = 0$, respectively, measured along the line $l^{(j)}$. Additionally, $\xi_{2k-1}^{(j)}$ and $\xi_{2k}^{(j)}$ are variables whose value is either -1 or 1 depending on the sign of the dot product $\boldsymbol{\alpha}_k^T \boldsymbol{\alpha}_{i^{(j)}}$. It should be recalled that eqs. (22) to (25) were deduced under the assumption that $\boldsymbol{\alpha}_k^T \boldsymbol{\alpha}_{i^{(j)}} \neq 0$. However, these expressions can be generalized for the case where $\boldsymbol{\alpha}_k^T \boldsymbol{\alpha}_{i^{(j)}} = 0$, as shown in detail in Appendix A.

The characterization of the indicator function associated with the k-th component as shown in eq. (21) allows a straightforward estimation of the sought line integral. For that purpose, let $\left\{q_1^{(j)}, q_2^{(j)}, \ldots, q_{2n_c}^{(j)}\right\}$ denote the sequence of integers such that $c_{q_1^{(j)}}^{(j)} \leq c_{q_2^{(j)}}^{(j)} \leq \ldots \leq c_{q_{2n_c}^{(j)}}^{(j)}$; in

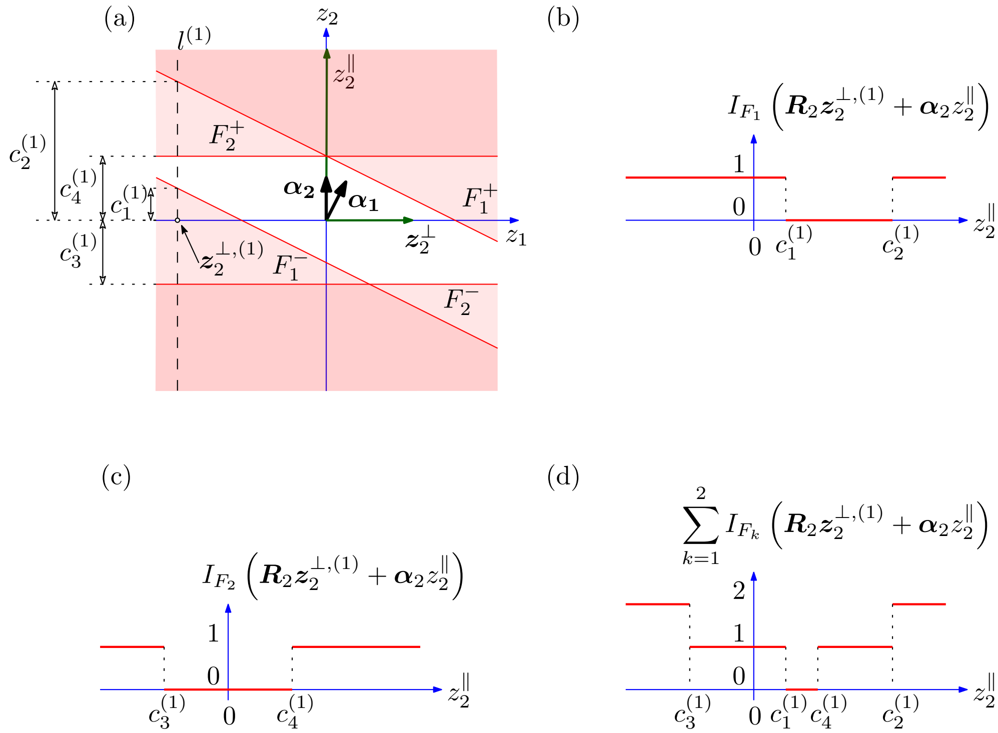

Figure 6: Schematic representation of line associated with the application of multidomain Line Sampling ($n = n_c = 2$). (a) Representation in standard Gaussian space. (b) Behavior of indicator function associated with the first component $I_{F_1}(\cdot)$ with respect to $z_2^{\|}$ along line $l^{(1)}$. (c) Behavior of indicator function associated with the second component $I_{F_2}(\cdot)$ with respect to $z_2^{\|}$ along line $l^{(1)}$. (d) Behavior of the compound indicator function with respect to $z_2^{\|}$ along line $l^{(1)}$.

addition, let $c^{(j)}_{q_0^{(j)}} \to -\infty$ and $c^{(j)}_{q_{2n_c+1}^{(j)}} \to \infty$. Furthermore, let $m_s^{(j)}$ be a natural number (including 0), which is defined as:

$$m_s^{(j)} = m_0^{(j)} + \sum_{l=1}^{s} \xi^{(j)}_{q_s^{(j)}},\ s = 0, \ldots, 2n_c,\ j = 1, \ldots, N \tag{26}$$

where $m_0^{(j)}$ counts the number of times that $\xi_q^{(j)} = -1, q = 1, \ldots, 2n_c$. The role of $m_s^{(j)}$, $s = 0, \ldots, 2n_c$ is expressing the number of components that fail at a point that belongs to the line $l^{(j)}$ and whose coordinate $z^{\|}_{i^{(j)}}$ lies within the interval $\left(c^{(j)}_{q_s^{(j)}}, c^{(j)}_{q_{s+1}^{(j)}}\right)$. In other words, $m_s^{(j)}$, $s = 0, \ldots, 2n_c$ contains all the values that the function $\sum_{k=1}^{n_c} I_{F_k}\left(\boldsymbol{R}_{i^{(j)}} \boldsymbol{z}^{\perp,(j)}_{i^{(j)}} + \boldsymbol{\alpha}_{i^{(j)}} z^{\|}_{i^{(j)}}\right)$ assumes along the line $l^{(j)}$. For a better understanding of this point, consider Figure 6(d) that illustrates the function $\sum_{k=1}^{n_c} I_{F_k}\left(\boldsymbol{R}_{i^{(j)}} \boldsymbol{z}^{\perp,(j)}_{i^{(j)}} + \boldsymbol{\alpha}_{i^{(j)}} z^{\|}_{i^{(j)}}\right)$ associated with line $l^{(1)}$ of Figure 6(a). It is seen that this function presents a staircase pattern, as depending on the value of $z_2^{\|}$, the number of failed components varies between 0, 1 and 2. This staircase pattern is reproduced by the quantity $m_s^{(j)}$ in eq. (26), as shown in Table 1. Note that for preparing this Table and according to the qualitative information in Figures 6(b) and 6(c), it is considered that $c_3^{(1)} < c_1^{(1)} < c_4^{(1)} < c_2^{(1)}$, $\xi_1^{(1)} = \xi_3^{(1)} = -1$ and $\xi_2^{(1)} = \xi_4^{(1)} = 1$.

s	$q_s^{(1)}$	$\xi_{q_s^{(1)}}^{(1)}$	$\left(c_{q_s^{(1)}}^{(1)}, c_{q_{s+1}^{(1)}}^{(1)}\right)$	$m_s^{(1)}$
0	-	-	$\left(-\infty, c_3^{(1)}\right)$	-2
1	3	-1	$\left(c_3^{(1)}, c_1^{(1)}\right)$	-1
2	1	-1	$\left(c_1^{(1)}, c_4^{(1)}\right)$	0
3	4	1	$\left(c_4^{(1)}, c_2^{(1)}\right)$	1
4	2	1	$\left(c_2^{(1)}, \infty\right)$	2

Table 1: Values that variable $m_s^{(1)}$ assumes along line $l^{(1)}$ associated with the schematic illustration in Figure 6.

Taking into account the above definitions, eq. (16) is calculated in closed form as shown below:

$$p_{i^{(j)}}\left(\boldsymbol{z}_{i^{(j)}}^{\perp,(j)}\right) = \sum_{s=0}^{s^L-1} \frac{\Phi\left(c_{q_{s+1}^{(j)}}^{(j)}\right) - \Phi\left(c_{q_s^{(j)}}^{(j)}\right)}{m_s^{(j)}} + \sum_{s=s^U}^{2n_c} \frac{\Phi\left(c_{q_{s+1}^{(j)}}^{(j)}\right) - \Phi\left(c_{q_s^{(j)}}^{(j)}\right)}{m_s^{(j)}} \tag{27}$$

where s^L is an integer such that $c_{q_{s^L}^{(j)}}^{(j)} = -\beta_{i^{(j)}}^L$ and s^U is another integer such that $c_{q_{s^U}^{(j)}}^{(j)} = \beta_{i^{(j)}}^U$. It is noted that from a numerical viewpoint, the computation of eq. (27) demands evaluating the response of each of the components twice, as it is necessary to solve two dot products involving the unit vector $\boldsymbol{\alpha}_l$ (see eqs. (22) to (25)). Therefore, assessing the estimator $\tilde{p}_F$ in eq. (15) demands $2N$ evaluations of each component response.

3.4. Summary

The application of multidomain Line Sampling for calculating the failure probability of a series system as considered in this contribution involves the following steps.

1. Define the basic information of the problem. This implies setting up the probabilistic characterization of the parameter vector $\boldsymbol{x}$ (of dimension n) in terms of its mean $\boldsymbol{\mu}$ and (positive definite) covariance matrix $\boldsymbol{C}$. Additionally, define vector $\boldsymbol{a}_i,\ i = 1, \ldots, n_c$ that characterizes the response of the i-th component as well as the allowable lower and upper bounds for the response (b_i^L and b_i^U, respectively).
2. Set up the performance functions in standard normal space by applying eqs. (1), (2) and (3). Calculate the reliability indexes β_i^L and $\beta_i^U,\ i = 1, \ldots, n_c$ as well as the unit vectors $\boldsymbol{\alpha}_i, i = 1, \ldots, n_c$.

3. Calculate the weights $\omega_i,\ i = 1, \ldots, n_c$ by means of eq. (14).
4. Sample (with replacement) a total of N integers $i^{(j)},\ j = 1, \ldots, N$ from the set $I = \{1, 2, \ldots, n_c\}$ with probability $\omega_i,\ i = 1, \ldots, n_c$. Generate samples $\boldsymbol{z}_{i(j)}^{\perp,(j)},\ j = 1, \ldots, N$ applying the procedure described in Section 3.3.1 (see eq. (18)).
5. Estimate $p_{i(j)}\left(\boldsymbol{z}_{i(j)}^{\perp,(j)}\right),\ j = 1, \ldots, N$ by means of eq. (27).
6. Calculate the estimator of the failure probability as well as its coefficient of variation applying eqs. (15) and (17).

4. Examples

4.1. *Test Example 1*

This first test example is borrowed from [15, 43]. It comprises the calculation of the failure probability of a series system, where the response of its i-th component is defined as:

$$r_i(\boldsymbol{x}) = x_i,\ i = 1, \ldots, n_c \tag{28}$$

where x_i is a realization of a Gaussian random variable with zero mean, unit standard deviation and pairwise correlation coefficient 0.5 with all random variables (other than itself). That is, the correlation matrix $\boldsymbol{R}$ of dimension $n_c \times n_c$ is defined as:

$$\boldsymbol{R} = \begin{bmatrix} 1 & 0.5 & \ldots & 0.5 \\ 0.5 & 1 & \ldots & 0.5 \\ \vdots & \vdots & \ddots & \vdots \\ 0.5 & 0.5 & \ldots & 1 \end{bmatrix} \tag{29}$$

Note that there are $n = n_c$ random variables. The threshold levels associated with the performance of each component are set such that $b_i^L \to -\infty,\ i = 1, \ldots, n_c$ and $b_i^U = \beta,\ i = 1, \ldots, n_c$ (where β is a real number), respectively. The failure probability associated with this series system can be expressed in terms of the following one-dimensional integral [15, 43], which can be accurately calculated by means of an appropriate quadrature.

$$p_F = \int_{-\infty}^{\infty} \left(1 - \left(1 - \Phi\left(\frac{-\beta - \sqrt{0.5}z}{\sqrt{1 - 0.5}}\right)\right)^{n_c}\right) f_Z(z) dz \tag{30}$$

From the above equation, recall that $f_Z(\cdot)$ and $\Phi(\cdot)$ represent the probability density function and cumulative density function of a standard Gaussian random variable, respectively.

The problem described above is solved by means of both the above integral and multidomain Line Sampling. Different combinations of the number of components n_c (10^1, 10^2, 10^3, 10^4) and of the threshold β (3, 4, 5) are investigated. For all these combinations, multidomain Line Sampling is implemented considering $N = 200$ lines (hence, $2 \times 200 = 400$ system analyses are performed). The results obtained for the failure probability estimates as well as their coefficient of variation are shown in Figures 7 and 8, respectively.

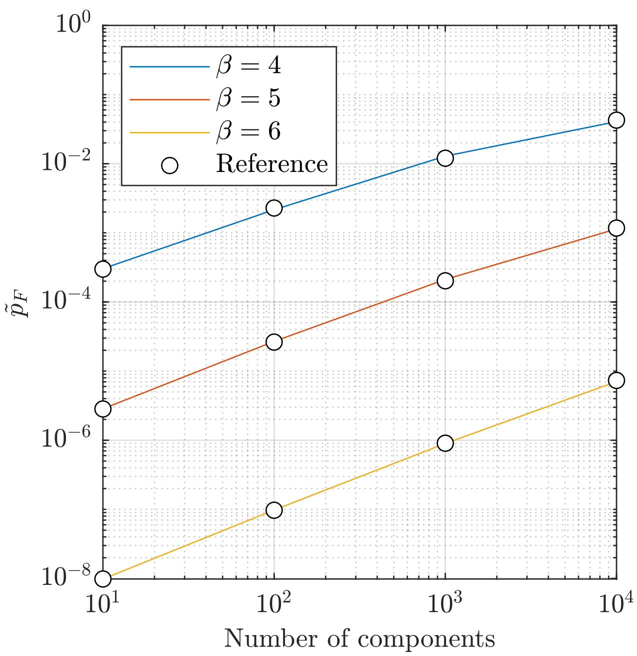

Figure 7: Example 1 - failure probability with respect to the number of components n_c and threshold level β. Solid line: estimates with multidomain Line Sampling. Circle: reference result.

Figure 7 illustrates the estimates of the failure probability generated with multidomain Line Sampling with solid line. In addition, the reference results provided by solving numerically the integral in eq. (30) are shown with circles. It is seen that there is an excellent agreement between the results, irrespective of the number of components and the threshold level. This is quite remarkable, as the failure probabilities involved in the figure span about six orders of magnitude.

Figure 8 shows the coefficient of variation associated with the estimates of the failure probability associated with multidomain Line Sampling. It is observed that all coefficients of variation are relatively low, which is quite desirable from a practical viewpoint. Furthermore, it is observed that the coefficients of variation are quite small for small values of failure probabilities. Such

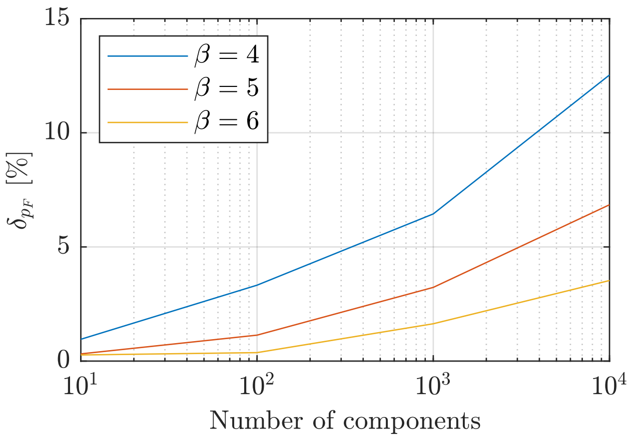

Figure 8: Example 1 - coefficient of variation of the failure probability with respect to the number of components n_c and threshold level β.

behavior is similar to the one observed in [29] and is explained by the fact that for small failure probabilities, interactions between components in the failure region become less relevant.

As a summary of this test example, it is observed that multidomain Line Sampling allows coping with a large number of random variables and components for estimating small failure probabilities with high precision and a reduced number of samples.

4.2. Test Example 2: Truss Structure

This test example involves a statically determined truss structure subject to three point loads $P_k,\ k = 1, \ldots, 3$, as depicted in Figure 9. These three point loads are modeled as Gaussian random variables with expected value 10 [kN], standard deviation 1 [kN] and constant correlation between them equal to 0.5. The maximum axial load that can be supported by the bars of the truss is as follows: bars 1, 4, 5, 6, 7, 8, 9 support a maximum load of 19 [kN]; bars 2 and 3 support a maximum load of 25 [kN]; bars 10 and 13 support a maximum load of 27 [kN]; and bars 11 and 12 support a maximum load of 10 [kN]. For simplicity, it is assumed that the bars are capable to support this maximum load either in tension or in compression.

The objective is determining the probability that the maximum allowable axial load due to the external loading is exceeded in one or more bars of the truss. As the truss possesses 13 bars and failure of any of these bars leads to failure of the system, this can be interpreted a series system with $n_c = 13$ components. The response of each component is its axial load and the allowable threshold is given by the maximum load supported by each bar.

The probability of failure associated with the series event is estimated by means of multidomain Line Sampling (mLS), considering a total of $N = 5 \times 10^5$ samples. As each sample comprises

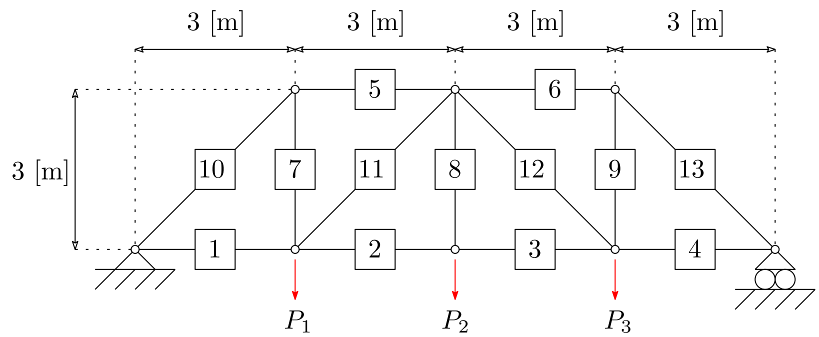

Figure 9: Example 2 - truss structure.

a total of two evaluations of the response of the components, a total of 10^6 system analyses are carried out. Note that this large number of samples for mLS is considered in order to carry out comparisons with Monte Carlo simulation, which provides reference results. In this case, Monte Carlo simulation is applied considering a total of 10^6 samples. The results obtained for the estimates of the failure probability and its coefficient of variation are shown in figures 10 and 11, respectively.

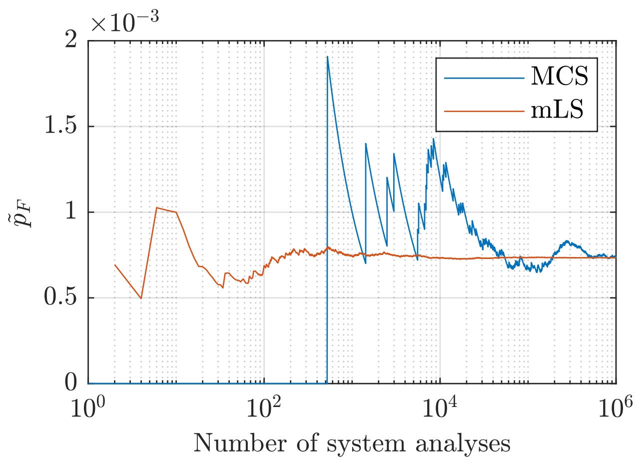

Figure 10: Example 2 - evolution of estimate of failure probability with respect to the number of system analyses (MCS: Monte Carlo simulation, mLS: multidomain Line Sampling).

An examination of Figure 10 indicates that both multidomain Line Sampling and Monte Carlo simulation provide similar estimates of the failure probability for a large number of system analyses. However, the estimator produced with multidomain Line Sampling stabilizes extremely fast: in fact, with about only 100 system analyses, it provides an excellent estimator of the failure probability. This is quite remarkable, considering that the failure probability is relatively small, that is, about $p_F \approx 7 \times 10^{-4}$.

The evolution of the coefficient of variation as shown in Figure 11 reinforces the conclusions

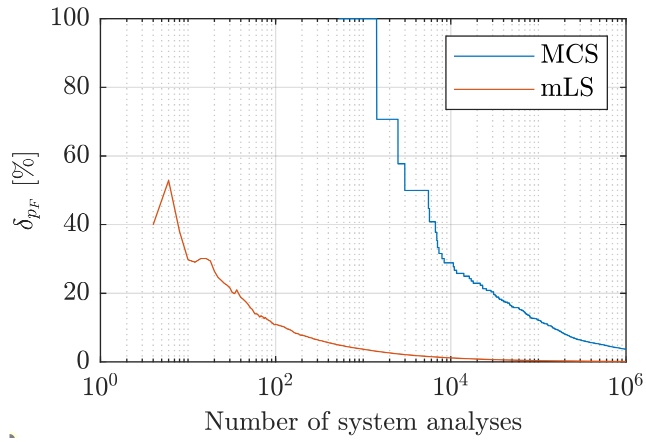

Figure 11: Example 2 - evolution of estimate of the coefficient of variation of the failure probability with respect to the number of system analyses (MCS: Monte Carlo simulation, mLS: multidomain Line Sampling).

drawn from Figure 10. It is seen that the coefficient of variation of the probability estimate produced with mLS is about 10% with only 100 system analyses. In order to produce an estimate with comparable coefficient of variation, Monte Carlo simulation demands 10^5 system analyses. Such result highlights the benefits of mLS for estimating failure probabilities associated with a series event.

4.3. Application Example 3: Six-Story Building Subject to Stochastic Gaussian Ground Acceleration

This application example involves a six-story reinforced concrete building subject to a stochastic Gaussian ground acceleration, as illustrated in Figure 12. The objective is estimating the first excursion probability that the interstory drifts of the building exceed a prescribed threshold within the duration of the acceleration. It is assumed that the building experiences small vibrations and hence, its behavior can be modeled as linear elastic. In fact, as discussed in the sequence, this problem can be modeled as a series system with a large number of components arising due to the discretization of time.

The assumption of linear elastic behavior of the building is appropriate for analyzing serviceability conditions, see e.g. [44, 45, 46], and allows conducting a reliability analysis by means of multidomain Line Sampling. For those cases where the assumption of a linear elastic behavior does not hold (e.g. progressive collapse or collapse), other more general methods should be applied, see e.g. [47, 48, 49, 50, 51].

Each floor of the building is composed of a square slab of side 32 [m] and thickness 0.2 [m], and is supported by 16 columns of square cross section of 0.4 [cm] and a shear wall of 0.2 [m] thickness.

The building is modeled as linear elastic and classically damped, with Young's modulus is equal to 2.3×10^{10} [Pa]. It is assumed that the building experiences small displacements and hence, its elements remain within the linear elastic range. The finite element model, which is taken from [52], involves about 9500 shell and beam elements and more than 50×10^3 degrees-of-freedom. Classical damping of 5% is considered for all modes retained in the analysis.

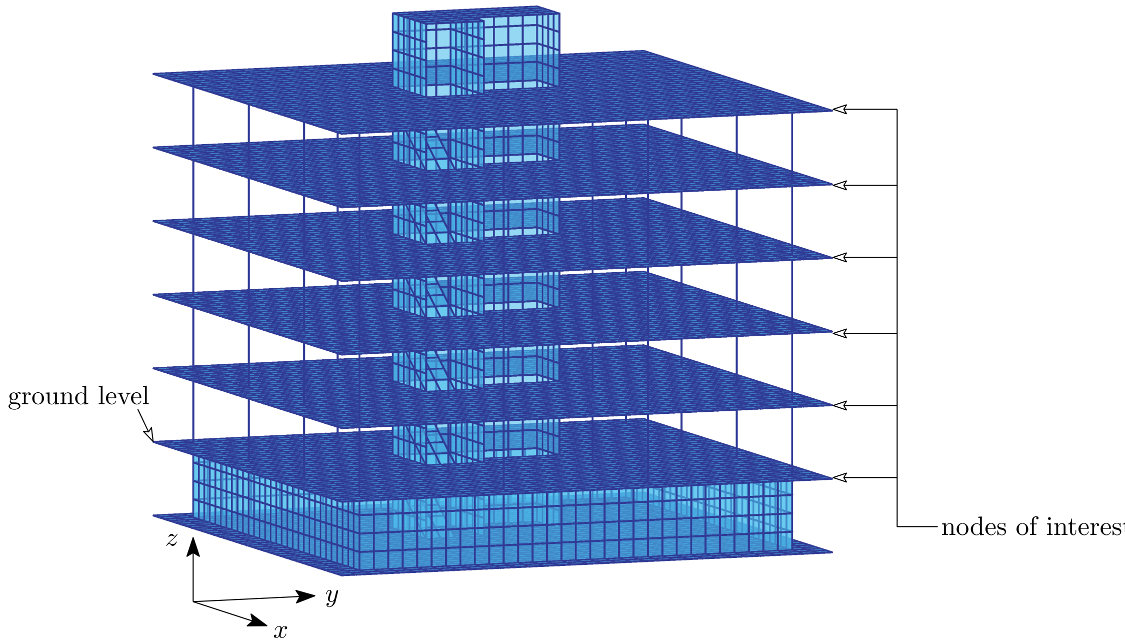

Figure 12: Example 3 - building model.

The building is excited by a stochastic Gaussian ground acceleration along the y direction (see Figure 12), which is modeled by means of the Clough-Penzien power spectrum (see, e.g. [53, 54, 55]), and which is in turn modulated by the Shinozuka-Sato envelope function [56]. The stochastic ground acceleration possesses a duration of 20 [s], with discrete representation considering a time step of 0.01 [s]. The associated discrete white noise process possesses spectral intensity of 3×10^{-4} [m^2/s^3] and the properties of the primary and secondary Clough-Penzien filters are circular frequency $\omega_1 = 4\pi$ [rad/s] and $\omega_2 = 0.4\pi$ [rad/s] and damping ratios $\zeta_1 = \zeta_2 = 0.7$, respectively. The parameters for the Shinozuka-Sato envelope are selected as $c_1 = 0.14$ and $c_2 = 0.16$. The stochastic ground acceleration is represented with the help of the Karhunen-Loève expansion considering 1466 terms (see, e.g. [57]). For additional details on the representation of the stochastic ground acceleration model, it is referred to [53, 54, 55, 56].

For design purposes, the interstory drifts along the y direction should not exceed a threshold level of 2×10^{-3} times the story height within the duration of the stochastic loading. This condition is verified considering the six nodes indicated in Figure 12, which implies that a total of five interstory drifts must be controlled. Appendix B provides a brief description on the procedure for calculating these interstory drifts. The chances that any of these interstory drifts exceed its prescribed threshold within the duration of the stochastic ground acceleration can be interpreted as the probability of failure of a series event, see e.g. [29]. In this case, the components are each of the interstory drifts responses at each time instant. As there is a total of five interstory drifts and 2001 discrete time instants, the total number of components is $n_c = 10005$. On the other hand, the total number of random variables involved in the problem is $n = 1466$, which is equal to the number of terms associated with the Karhunen-Loève expansion. Hence, the problem under consideration corresponds to a case with a large number of random variables (over 10^3 of them) and a large number of components (over 10^4 components).

The probability of failure associated with the system event is calculated by means of multidomain Line Sampling, considering a total of $N = 5\times10^3$ samples. This implies that the system's response is calculated a total of 10^4 times. That is, 10^4 dynamic analyses are carried out. In addition and in order to provide a basis for comparison, the failure probability is also assessed by means of Efficient Importance Sampling [29] and Directional Importance Sampling [31, 32], which are simulation techniques specially developed for calculating failure probabilities of linear structural systems subject to Gaussian excitation. These two simulation techniques are implemented considering a total of 10^4 samples (which imply performing a total of 10^4 dynamic analyses). The results obtained are shown in Figures 13 and 14 as well as in Table 2.

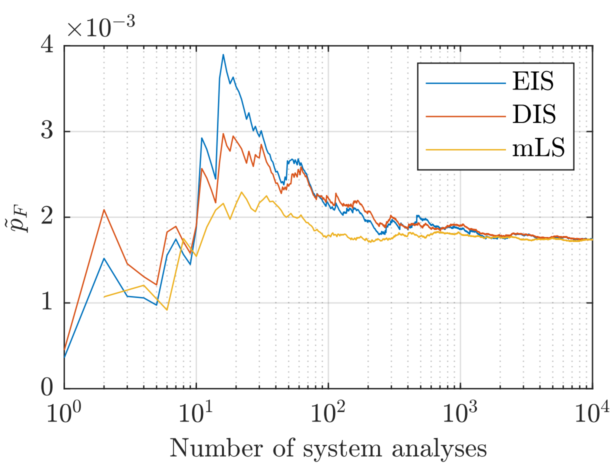

Figure 13: Example 3 - evolution of estimate of failure probability with respect to the number of system analyses (EIS: Efficient Importance Sampling, DIS: Directional importance Sampling, mLS: multidomain Line Sampling).

As noted from Figure 13, the three simulation techniques under consideration can produce good estimates of the failure probability with a reduced number of samples. However, it is seen that the estimator associated with multidomain Line Sampling stabilizes quicker than the estimators associated with the other two simulation techniques. In fact, with about $N = 50$ samples (that is, 100 system analyses), multidomain Line Sampling already provides an excellent estimate of the failure probability. This is confirmed by examining the results in table 2, where it is seen that the associated coefficient of variation is already below 10%.

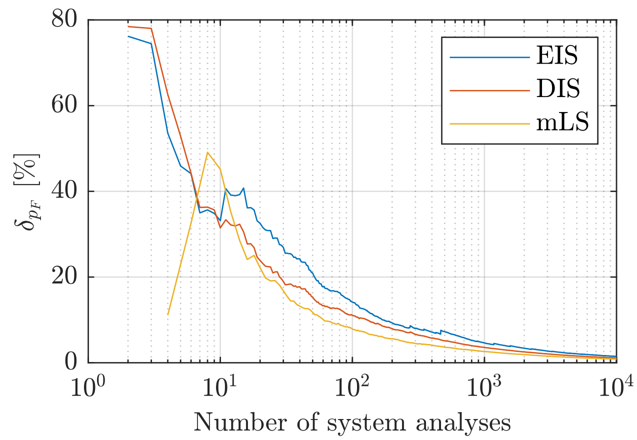

Figure 14: Example 3 - evolution of estimate of the coefficient of variation of the failure probability with respect to the number of system analyses (EIS: Efficient Importance Sampling, DIS: Directional importance Sampling, mLS: multidomain Line Sampling).

The results presented in Figure 14 support the observations already drawn from Figure 13. That is, the coefficient of variation associated with the probability estimates of all simulation techniques decreases quickly with the number of system analysis. Furthermore, the estimate associated with multidomain Line Sampling is the one presenting the smallest coefficient of variation (excluding the region of about 10 system analyses).

No. system analyses	$\tilde{p}_F^{\text{EIS}}$	$\delta_{p_F^{\text{EIS}}}$ [%]	$\tilde{p}_F^{\text{DIS}}$	$\delta_{p_F^{\text{DIS}}}$ [%]	$\tilde{p}_F^{\text{mLS}}$	$\delta_{p_F^{\text{mLS}}}$ [%]
10^2	2.2×10^{-3}	14.2%	2.2×10^{-3}	11.1%	1.8×10^{-3}	7.9%
10^3	1.9×10^{-3}	4.6%	1.9×10^{-3}	3.6%	1.8×10^{-3}	2.6%
10^4	1.7×10^{-3}	1.5%	1.7×10^{-3}	1.1%	1.7×10^{-3}	0.9%

Table 2: Example 3 - Estimates of the failure probability $\tilde{p}_F$ and its coefficient of variation δ_{p_F} (EIS: Efficient Importance Sampling, DIS: Directional importance Sampling, mLS: multidomain Line Sampling).

Table 2 reports the probability estimates and their coefficient of variation for the three simulation techniques under consideration for different number of system analyses. It is seen that all three techniques are quite successful in estimating the failure probability, as there is good agreement between the different estimates, with relatively low coefficient of variation. However, for all cases reported in the table, multidomain Line Sampling provides probability estimates which are closer to the reference solution (with 10^4 system analyses) and with the smallest coefficient of variation.

The (small) differences in performance between the three simulation techniques analyzed in this example as presented in Table 2 can be understood as follows. Efficient Importance Sampling (EIS) is a specially-designed variant of Importance Sampling that estimates the failure probability by generating samples (realizations of $\boldsymbol{Z}$) exclusively in the failure domain. Directional Importance Sampling (DIS) operates in a similar way as Efficient Importance Sampling, but it explores directions instead of samples; in other words, it explores an infinite number of samples along a given ray starting at the origin of the standard normal space. Multidomain Line Sampling (mLS) shares some common aspects with Directional Importance Sampling in the sense that an infinite number of samples is explored. However, these samples fall in a line whose orientation is different from the aforementioned ray.

As a further comparison between the performance of the three simulation techniques discussed above, Table 3 presents both the number of system analyses and the relative execution time for attaining an estimate of the failure probability with coefficient of variation $\delta_{p_F} = 10\%$. It is observed that the smallest number of system analyses and relative execution time are associated with mLS. The other two simulation approaches, that is EIS and DIS, demand more samples to attain the prescribed coefficient of variation and more relative execution time than those associated with mLS. An an additional observation from Table 3, it should be noted that the relation between number of system analyses and relative execution time for the different simulation techniques is not proportional, as the specific implementation steps of EIS [29], DIS [31, 32] and mLS differ between them.

Simulation technique	No. system analyses	Relative Execution time
EIS	171	249%
DIS	130	234%
mLS	62	100%

Table 3: Example 3 - Number of system analyses and relative execution time for achieving probability estimate with coefficient of variation of 10% (EIS: Efficient Importance Sampling, DIS: Directional importance Sampling, mLS: multidomain Line Sampling).

5. Conclusions and Outlook

This contribution has presented an approach for estimating the probability of occurrence of a series system event by means of multidomain Line Sampling. In particular, multidomain Line Sampling is applied in order to determine the *effective* contribution of a single component to the overall failure probability. In this context, *effective* means that proper consideration is given to the failure event associated with a particular component and its interaction with other components. The overall failure probability is then determined by randomly sampling among different components. The examples presented in this contribution suggest that multidomain Line Sampling is applicable to problems involving both a small and a large number of random variables and components, respectively.

Much of the success of the multidomain Line Sampling strategy as reported herein can be attributed to the way each failure domain associated with an individual component is examined. By exploring lines, one can analyze an infinite number of realizations instead of a single one. In this way, each line provides a considerable amount of information. Moreover, in view of the linearity of the response with respect to the unknown random parameters, it is possible to solve the integral associated with that line by means of a closed-form, analytic formula.

While the results presented are encouraging, several issues deserve further research. One line of possible development involves extending the capabilities of multidomain Line Sampling in order to account for problems that involve either non Gaussian random variables or responses which are non linear with respect to the unknown random parameters. Preliminary research efforts conducted by the authors suggest that such an extension is feasible applying a so-called smooth indicator function, as suggested in [58, 59, 60]. Another path for development considers the extension of multidomain Line Sampling for the analysis of problems involving parallel systems or more general configurations. In particular, for the case of parallel systems, the results reported in [19] could serve as a basis.

6. Acknowledgments

This research is partially supported by ANID (National Agency for Research and Development, Chile) under its program FONDECYT, grant number 1180271 and the National Natural Science Foundation of China (NSFC) under grant number NSFC 51905430. The first author developed part of this work during a research stay at the Institute for Risk and Reliability (IRZ) of the Leibniz

Universität Hannover, Germany. Both the first and second authors conducted this research under the auspice of the *Alexander von Humboldt Foundation*. This support is gratefully acknowledged by the authors.

Appendix A. Calculation of $\boldsymbol{c}_{\boldsymbol{2k-1}}^{(j)}$, $\boldsymbol{c}_{\boldsymbol{2k}}^{(j)}$, $\boldsymbol{\xi}_{\boldsymbol{2k-1}}^{(j)}$ and $\boldsymbol{\xi}_{\boldsymbol{2k}}^{(j)}$

The scheme for evaluating the line integral associated with the implementation of multidomain Line Sampling as presented in Section 3.3.2 requires few modifications for its implementation in case $\boldsymbol{\alpha}_k^T \boldsymbol{\alpha}_{i^{(j)}} = 0$. To motivate the discussion, consider the schematic representation in Figure A.15, that depicts a particular case where $n = n_c = 2$, $N = 3$ and $i^{(1)} = i^{(2)} = i^{(3)} = 2$.

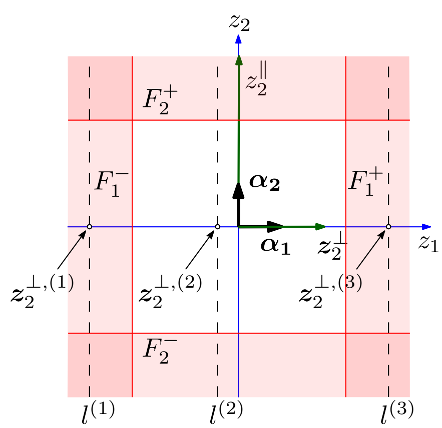

Figure A.15: Schematic representation of line associated with the application of multidomain Line Sampling in case $\boldsymbol{\alpha}_k^T \boldsymbol{\alpha}_{i^{(j)}} = 0$ ($n = n_c = 2$).

As noted from Figure A.15, it is seen that component 1 fails for all points that belong to lines $l^{(1)}$ and $l^{(3)}$; on the contrary, it is seen that line $l^{(2)}$ never intersects the failure domain associated with component 1. Taking into account these observations and recalling the structure of eq. (21), it is concluded that for the case where $\boldsymbol{\alpha}_k^T \boldsymbol{\alpha}_{i^{(j)}} = 0$, the unit step functions do not depend on $z_{i^{(j)}}^{\parallel}$ and that the Euclidean distances $c_{2k-1}^{i^{(j)}}$ and $c_{2k-1}^{i^{(j)}}$ must tend to either minus infinity or plus infinity in order to reflect that failure occurs or not with respect to the k-th component along line $l^{(j)}$. It is straightforward to demonstrate that the definitions for the distances $c_{2k-1}^{i^{(j)}}$ and $c_{2k-1}^{i^{(j)}}$ as presented in eqs. (22) and (23) must be extended as shown below in order to accommodate the case where $\boldsymbol{\alpha}_k^T \boldsymbol{\alpha}_{i(j)} = 0$.

$$c_{2k-1}^{(j)} = \begin{cases} -\infty & \text{if } \boldsymbol{\alpha}_k^T \boldsymbol{\alpha}_{i(j)} = 0 \wedge \beta_k^L + \boldsymbol{\alpha}_k^T \boldsymbol{R}_{i(j)} \boldsymbol{z}_{i(j)}^{\perp,(j)} \leq 0 \\ -\frac{\beta_k^L + \boldsymbol{\alpha}_k^T \boldsymbol{R}_{i(j)} \boldsymbol{z}_{i(j)}^{\perp,(j)}}{\boldsymbol{\alpha}_k^T \boldsymbol{\alpha}_{i(j)}} & \text{if } \boldsymbol{\alpha}_k^T \boldsymbol{\alpha}_{i(j)} \neq 0 \\ \infty & \text{if } \boldsymbol{\alpha}_k^T \boldsymbol{\alpha}_{i(j)} = 0 \wedge \beta_k^L + \boldsymbol{\alpha}_k^T \boldsymbol{R}_{i(j)} \boldsymbol{z}_{i(j)}^{\perp,(j)} > 0 \end{cases}, \ k = 1, \ldots, n_c, \ j = 1, \ldots, N \tag{A.1}$$

$$c_{2k}^{(j)} = \begin{cases} -\infty & \text{if } \boldsymbol{\alpha}_k^T \boldsymbol{\alpha}_{i(j)} = 0 \wedge \beta_k^U - \boldsymbol{\alpha}_k^T \boldsymbol{R}_{i(j)} \boldsymbol{z}_{i(j)}^{\perp,(j)} \leq 0 \\ \frac{\beta_k^U - \boldsymbol{\alpha}_l^T \boldsymbol{R}_{i(j)} \boldsymbol{z}_{i(j)}^{\perp,(j)}}{\boldsymbol{\alpha}_k^T \boldsymbol{\alpha}_{i(j)}} & \text{if } \boldsymbol{\alpha}_k^T \boldsymbol{\alpha}_{i(j)} \neq 0 \\ \infty & \text{if } \boldsymbol{\alpha}_k^T \boldsymbol{\alpha}_{i(j)} = 0 \wedge \beta_k^U - \boldsymbol{\alpha}_k^T \boldsymbol{R}_{i(j)} \boldsymbol{z}_{i(j)}^{\perp,(j)} > 0 \end{cases}, \ k = 1, \ldots, n_c, \ j = 1, \ldots, N \tag{A.2}$$

The definition of the variables $\xi_{2k-1}^{(j)}$ and $\xi_{2k}^{(j)}$ as presented in eqs. (24) and (25) must be modified as well in order to accommodate the case where $\boldsymbol{\alpha}_k^T \boldsymbol{\alpha}_{i(j)} = 0$. It can be demonstrated that such modification leads to:

$$\xi_{2k-1}^{(j)} = \begin{cases} 1 & \text{if } \boldsymbol{\alpha}_k^T \boldsymbol{\alpha}_{i(j)} \leq 0 \\ -1 & \text{otherwise} \end{cases}, \ k = 1, \ldots, n_c, \ j = 1, \ldots, N \tag{A.3}$$

$$\xi_{2k}^{(j)} = \begin{cases} 1 & \text{if } \boldsymbol{\alpha}_k^T \boldsymbol{\alpha}_{i(j)} \geq 0 \\ -1 & \text{otherwise} \end{cases}, \ k = 1, \ldots, n_c, \ j = 1, \ldots, N \tag{A.4}$$

Equations (A.1) to (A.4) as presented above allow calculating the line integral associated with multidomain Line Sampling following the steps described in Section 3.3.2. In this sense, it is noted that no modifications are required for eqs. (26) and (27) for the case where $\boldsymbol{\alpha}_k^T \boldsymbol{\alpha}_{i(j)} = 0$.

Appendix B. Calculation of Interstory Drifts

The interstory drifts are calculated by means of the convolution integral, taking advantage of the linearity of the response with respect to the ground acceleration.

$$\eta_i(t, \boldsymbol{z}) = \int_0^t h_i(t - \tau)\, p(\tau, \boldsymbol{z})\, d\tau, \ i = 1, \ldots, n_\eta \tag{B.1}$$

In the above equation, η_i represents the i-th interstory drift, h_i is the corresponding unit impulse response function and p represents the ground acceleration, which depends both on time t and a realization $\boldsymbol{z}$ of the standard Gaussian distribution. For the case considered in this contribution, the unit impulse response function is:

$$h_i(t) = \sum_{v=1}^{n_\phi} \frac{\boldsymbol{\kappa}_v^T \boldsymbol{\phi}_v \boldsymbol{\phi}_v^T \boldsymbol{\rho}}{\boldsymbol{\phi}_v^T \boldsymbol{M} \boldsymbol{\phi}_v} \frac{1}{\omega_{d,v}} e^{-\zeta_v \omega_{n,v} t} \sin(\omega_{d,v} t),\ i = 1, \ldots, n_\eta \tag{B.2}$$

where $\boldsymbol{\kappa}_v,\ i = 1, \ldots, n_\eta$ is a vector that couples the degrees-of-freedom of the model for calculating the intestory drifts; $\boldsymbol{\rho}$ is a vector that couples the ground acceleration with the degrees-of-freedom of the model; $\boldsymbol{\phi}_v,\ v = 1, \ldots, n_D$ are the eigenvectors associated with the eigenproblem of the undamped equation of motion involving the mass $\boldsymbol{M}$ and stiffness $\boldsymbol{K}$ matrices of the model; $\omega_{n,v},\ v = 1, \ldots, n_D$ are the natural frequencies of the system; $\zeta_v,\ v = 1, \ldots, n_D$ are the corresponding damping ratios; $\omega_{d,v} = \omega_{n,v}\sqrt{(1-\zeta_v^2)},\ v = 1, \ldots, n_D$ are the damped frequencies; and n_ϕ is the number of modes retained for modal analysis [61].

As the stochastic ground acceleration is represented by means of the Karhunen-Loève expansion, the interstory drift evaluated at discrete time instant t_k is approximated as:

$$\eta_i(t_k, \boldsymbol{z}) = \sum_{l=1}^{k} \Delta t \epsilon_l h_i(t_k - t_l) \boldsymbol{B}_{l:} \boldsymbol{z},\ i = 1, \ldots, n_\eta,\ k = 1, \ldots, n_T \tag{B.3}$$

where Δt is the time discretization; n_T is the total number of discrete time instants; $\boldsymbol{B}_{l:}$ denotes the l-th row of matrix $\boldsymbol{B}$ (see eq. (1)), and ϵ_l is a coefficient depending on the numerical integration scheme used in the evaluation of the convolution integral. In this particular case, ϵ_l is chosen according to the trapezoidal integration rule [62], yielding $\epsilon_l = 1/2$ if $l = 1$ or $l = k$; otherwise, $\epsilon_l = 1$. From eq. (B.3), it is straightforward to see that the i-th interstory drift at the k-th time instant can be represented in the form $\eta_i(t_k, \boldsymbol{z}) = \boldsymbol{a}_{i,k}^T \boldsymbol{z}$, where $\boldsymbol{a}_{i,k}$ is a vector of constant coefficients. Such representation matches with the type of problems considered in this contribution, where the response of interest is a linear combination of a number of parameters following a Gaussian distribution (see Section 2.1).

References

[1] M. Beer, S. Ferson, V. Kreinovich, Imprecise probabilities in engineering analyses, Mechanical Systems and Signal Processing 37 (1-2) (2013) 4–29.

[2] O. Ditlevsen, Narrow reliability bounds for structural systems, Journal of Structural Mechanics 7 (4) (1979) 453–472.

[3] Y. Zhang, High-order reliability bounds for series systems and application to structural systems, Computers & Structures 46 (2) (1993) 381 – 386.

[4] W. Fauriat, N. Gayton, AK-SYS: An adaptation of the AK-MCS method for system reliability, Reliability Engineering & System Safety 123 (2014) 137 – 144.

[5] Y. Jiang, L. Zhao, M. Beer, L. Wang, J. Zhang, Dominant failure mode analysis using representative samples obtained by multiple response surfaces method, Probabilistic Engineering Mechanics 59 (2020) 103005.

[6] K. Yuan, N.-C. Xiao, Z. Wang, K. Shang, System reliability analysis by combining structure function and active learning kriging model, Reliability Engineering & System Safety 195 (2020) 106734.

[7] P. Wei, F. Liu, C. Tang, Reliability and reliability-based importance analysis of structural systems using multiple response Gaussian process model, Reliability Engineering & System Safety 175 (2018) 183 – 195.

[8] X. Zhang, L. Wang, J. Sorensen, AKOIS: An adaptive kriging oriented importance sampling method for structural system reliability analysis, Structural Safety 82 (2020) 101876.

[9] J. Song, A. Der Kiureghian, Bounds on system reliability by linear programming, Journal of Engineering Mechanics 123 (6) (2003) 627–636.

[10] J. Song, W.-H. Kang, System reliability and sensitivity under statistical dependence by matrix-based system reliability method, Structural Safety 31 (2) (2009) 148 – 156.

[11] P. Wei, Z. Lu, L. Tian, Addition laws of failure probability and their applications in reliability analysis of structural system with multiple failure modes, Proceedings of the Institution of Mechanical Engineers, Part C: Journal of Mechanical Engineering Science 227 (1) (2013) 120–136.

[12] J.-E. Byun, J. Song, Bounds on reliability of larger systems by linear programming with delayed column generation, Journal of Engineering Mechanics 146 (4) (2020) 04020008.

[13] M. Hohenbichler, R. Rackwitz, First-order concepts in system reliability, Structural Safety 1 (3) (1983) 177–188.

[14] K. Roscoe, F. Diermanse, T. Vrouwenvelder, System reliability with correlated components: Accuracy of the equivalent planes method, Structural Safety 57 (2015) 53 – 64.

[15] W.-H. Kang, J. Song, Evaluation of multivariate normal integrals for general systems by sequential compounding, Structural Safety 32 (1) (2010) 35 – 41.

[16] R. Ambartzumian, A. Der Kiureghian, V. Ohaniana, H. Sukiasiana, Multinormal probability by sequential conditioned importance sampling: theory and application, Probabilistic Engineering Mechanics 13 (4) (1998) 299–308.

[17] A. Genz, Numerical computation of multivariate normal probabilities, Journal of Computational and Graphical Statistics 1 (2) (1992) 141–149.

[18] R. Melchers, Importance sampling in structural systems, Structural Safety 6 (1) (1989) 3–10.

[19] E. Patelli, H. Pradlwarter, G. Schuëller, On multinormal integrals by importance sampling for parallel system reliability, Structural Safety 33 (1) (2011) 1–7.

[20] H.-S. Li, T. Wang, J.-Y. Yuan, H. Zhang, A sampling-based method for high-dimensional time-variant reliability analysis, Mechanical Systems and Signal Processing 126 (2019) 505 – 520.

[21] C. Gong, D. Frangopol, An efficient time-dependent reliability method, Structural Safety 81 (2019) 101864.

[22] S. Kim, B. Ge, D. Frangopol, Effective optimum maintenance planning with updating based on inspection information for fatigue-sensitive structures, Probabilistic Engineering Mechanics 58 (2019) 103003.

[23] X. Yuan, S. Liu, M. Faes, M. Valdebenito, M. Beer, An efficient importance sampling approach for reliability analysis of time-variant structures subject to time-dependent stochastic load, Mechanical Systems and Signal Processing 159 (2021) 107699.

[24] A. Der Kiureghian, The geometry of random vibrations and solutions by FORM and SORM, Probabilistic Engineering Mechanics 15 (1) (2000) 81–90.

[25] S. Gupta, C. Manohar, Reliability analysis of randomly vibrating structures with parameter uncertainties, Journal of Sound and Vibration 297 (3) (2006) 1000 – 1024.

[26] S. Cho, First-order reliability analysis of slope considering multiple failure modes, Engineering Geology 154 (2013) 98–105.

[27] P. Zeng, R. Jimenez, An approximation to the reliability of series geotechnical systems using a linearization approach, Computers and Geotechnics 62 (2014) 304–309.

[28] W.-H. Kang, J. Song, P. Gardoni, Matrix-based system reliability method and applications to bridge networks, Reliability Engineering & System Safety 93 (11) (2008) 1584 – 1593.

[29] S. Au, J. Beck, First excursion probabilities for linear systems by very efficient importance sampling, Probabilistic Engineering Mechanics 16 (3) (2001) 193–207.

[30] L. Katafygiotis, S. Cheung, Domain decomposition method for calculating the failure probability of linear dynamic systems subjected to Gaussian stochastic loads, Journal of Engineering Mechanics 132 (5) (2006) 475–486.

[31] O. Ditlevsen, P. Bjerager, R. Olesen, A. Hasofer, Directional simulation in Gaussian processes, Probabilistic Engineering Mechanics 3 (4) (1988) 207 – 217.

[32] M. Misraji, M. Valdebenito, H. Jensen, C. Mayorga, Application of directional importance sampling for estimation of first excursion probabilities of linear structural systems subject to stochastic Gaussian loading, Mechanical Systems and Signal Processing 139 (2020) 106621.

[33] P. Koutsourelakis, H. Pradlwarter, G. Schuëller, Reliability of structures in high dimensions, part I: Algorithms and applications, Probabilistic Engineering Mechanics 19 (4) (2004) 409–417.

[34] E. Zio, The Monte Carlo Simulation Method for System Reliability and Risk Analysis, Springer London, 2013.

[35] G. Schuëller, H. Pradlwarter, Benchmark study on reliability estimation in higher dimensions of structural systems – An overview, Structural Safety 29 (2007) 167–182.

[36] G. Schuëller, H. Pradlwarter, P. Koutsourelakis, A critical appraisal of reliability estimation procedures for high dimensions, Probabilistic Engineering Mechanics 19 (4) (2004) 463–474.

[37] M. Hohenbichler, R. Rackwitz, Improvement of second-order reliability estimates by importance sampling, J. Engrg. Mech. Div., ASCE 114 (12) (1988) 2195–2199.

[38] B. Sudret, Uncertainty propagation and sensitivity analysis in mechanical models - contributions to structural reliability and stochastic spectral methods (Habilitation) (2007).

[39] M. F. Pellissetti, G. I. Schuëller, H. J. Pradlwarter, A. Calvi, S. Fransen, M. Klein, Reliability analysis of spacecraft structures under static and dynamic loading, Computers & Structures 84 (21) (2006) 1313–1325.

[40] P. Liu, A. Der Kiureghian, Multivariate distribution models with prescribed marginals and covariances, Probabilistic Engineering Mechanics 1 (2) (1986) 105–112.

[41] M. de Angelis, E. Patelli, M. Beer, Advanced line sampling for efficient robust reliability analysis, Structural Safety 52, Part B (2015) 170–182.

[42] G. Schuëller, R. Stix, A critical appraisal of methods to determine failure probabilities, Structural Safety 4 (4) (1987) 293–309.

[43] X.-X. Yuan, M. Pandey, Analysis of approximations for multinormal integration in system reliability computation, Structural Safety 28 (4) (2006) 361–377.

[44] D. García, M. Rosales, R. Sampaio, Dynamic behaviour of a timber footbridge with uncertain material properties under a single deterministic walking load, Structural Safety 77 (2019) 10 – 17.

[45] D. Honfi, A. Mårtensson, S. Thelandersson, Reliability of beams according to eurocodes in serviceability limit state, Engineering Structures 35 (2012) 48–54.

[46] M. Huang, C. Chan, W. Lou, Optimal performance-based design of wind sensitive tall buildings considering uncertainties, Computers & Structures 98-99 (2012) 7–16.

[47] S. Au, First passage probability of elasto-plastic systems by importance sampling with adapted process, Probabilistic Engineering Mechanics 23 (2-3) (2008) 114–124.

[48] S. Bansal, S. Cheung, On the evaluation of multiple failure probability curves in reliability analysis with multiple performance functions, Reliability Engineering & System Safety 167

(2017) 583–594, special Section: Applications of Probabilistic Graphical Models in Dependability, Diagnosis and Prognosis.

[49] F. Cadini, F. Santos, E. Zio, An improved adaptive kriging-based importance technique for sampling multiple failure regions of low probability, Reliability Engineering & System Safety 131 (2014) 109 – 117.

[50] W.-S. Liu, S. Cheung, W.-J. Cao, An efficient surrogate-aided importance sampling framework for reliability analysis, Advances in Engineering Software 135 (2019) 102687.

[51] K. Yuen, L. Katafygiotis, An efficient simulation method for reliability analysis of linear dynamical systems using simple additive rules of probability, Probabilistic Engineering Mechanics 20 (1) (2005) 109–114.

[52] E. Patelli, H. Panayirci, M. Broggi, B. Goller, P. Beaurepaire, H. Pradlwarter, G. Schuëller, General purpose software for efficient uncertainty management of large finite element models, Finite Elements in Analysis and Design 51 (2012) 31–48.

[53] T. Soong, M. Grigoriu, Random Vibration of Mechanical and Structural Systems, Prentice Hall, Englewood Cliffs, New Jersey, 1993.

[54] G. Fu, Seismic response statistics of SDOF system to exponentially modulated coloured input: An explicit solution, Earthquake Engineering & Structural Dynamics 24 (10) (1995) 1355–1370.

[55] A. Zerva, Spatial Variation of Seismic Ground Motions – Modeling and Engineering Applications, CRC Press, 2009.

[56] M. Shinozuka, Y. Sato, Simulation of nonstationary random process, Journal of the Engineering Mechanics Division 93 (1) (1967) 11–40.

[57] G. Stefanou, The stochastic finite element method: Past, present and future, Computer Methods in Applied Mechanics and Engineering 198 (9-12) (2009) 1031–1051.

[58] L. Katafygiotis, K. Zuev, Estimation of small failure probabilities in high dimensions by adaptive linked importance sampling, in: M. Papadrakakis, D. Charmpis, N. Lagaros, Y. Tsompanakis (Eds.), ECCOMAS Thematic Conference on Computational Methods in Structural Dynamics and Earthquake Engineering (COMPDYN), Rethymno, Crete, Greece, 2007.

[59] P. Beaurepaire, H. Jensen, G. Schuëller, M. Valdebenito, Reliability-based optimization using bridge importance sampling, Probabilistic Engineering Mechanics 34 (2013) 48–57.

[60] I. Papaioannou, K. Breitung, D. Straub, Reliability sensitivity estimation with sequential importance sampling, Structural Safety 75 (2018) 24 – 34.

[61] A. Chopra, Dynamics of structures: theory and applications to earthquake engineering, Prentice Hall, 1995.

[62] W. Gautschi, Numerical Analysis, 2nd Edition, Birkhäuser Boston, 2012.